CeO_2/Pt(111) interface studied using first-principles density functional theory calculations

Christian Spiel, Peter Blaha, Yuri Suchorski, Karlheinz Schwarz, and Günther Rupprechter
Institute of Materials Chemistry, Vienna University of Technology, AT-1060 Vienna, Austria
(Received 7 April 2011; published 6 July 2011)

In this contribution we present *ab initio* density-functional-theory (DFT) calculations for CeO_2 monolayers on the Pt(111) surface. The ceria surface and ceria-metal interface are of great interest because of the oxygen-storage and release capabilities of ceria, which are widely utilized in catalysis. Both the experimentally reported 3 : 4 [(4 × 4)] and 5 : 7 [(1.4 × 1.4)] matching geometries of the CeO_2/Pt(111) system are studied using the GGA + U exchange-correlation scheme. Geometry optimizations of the structures are performed, resulting in a significant corrugation of both the Pt surface as well as the ceria adlayer surface. The total energies and adsorption energies of three different adsorption geometries for the 3 : 4 type are compared to the 5 : 7 structure in terms of stability. The electronic properties and the bonding character are studied by analysis of the density of states (DOS) and of the electron density. The charge transfer occurring during adsorption is calculated using the atoms-in-molecules (AIM) method. Strong interactions are detected, which are mainly based on electrostatic interactions between the topmost Pt layer and the oxygen atoms at the interface, but also include small contributions from hybridization.

DOI: 10.1103/PhysRevB.84.045412 PACS number(s): 68.35.−p, 73.20.At

I. INTRODUCTION

Ceria (CeO_2) belongs to the class of so-called reducible oxides and is, among other applications, widely used in catalysis, e.g., as an additive in automotive catalysts. The $Ce^{3+} \rightarrow Ce^{4+}$ switch in the oxidation state of CeO_x enables oxygen storage compensating transient deviations from the stoichiometric air-to-fuel ratio during operation.[1] However, atomistic details on the (presumably, spill-over-mediated) oxygen-transport mechanism are still lacking despite intensive experimental and modeling efforts.[2]

Ceria is also known to promote the low-temperature oxidation of CO and hydrocarbons,[3] as well as the water-gas shift reaction on supported noble-metal catalysts.[4] Again, details of the promoting function are still not well understood. The complex interplay between, e.g., Pt, Ce, CO, and O species under reaction conditions is influenced by both electronic and structural contributions of the mutual ceria/noble-metal interaction.

The inherent complexity of technological catalysts, such as the size distribution of the catalyst nanoparticles, complex surface morphologies, the presence of structural defects, etc.,[5] hinders the use of surface science techniques to reveal the nature of the ceria/noble-metal interaction under catalytic reaction conditions. To get insight into these processes on a molecular level, well-defined planar model systems have been utilized, such as oxide-supported metal nanoparticles[6] or "inverse-supported catalysts,"[7,8] the latter being composed of a (single or polycrystalline) metal surface covered by small oxide islands.

Recently, such an inverse-model catalyst was created by growing well-defined monolayer CeO_x islands on a Pt(111) surface and the Ce oxidation state as well as the catalytic activity toward CO oxidation were simultaneously monitored *in situ*.[9,10] As compared to (pure) Pt(111), on the CeO_x-modified surface, strongly enhanced reactivity was observed (in addition to a remarkable shift of the bistable region of the reaction toward higher CO pressures). To explain the apparently local enhancement of catalytic activity, a concept of an electronically modified active border around the CeO_x islands (with a width of a few interatomic distances, i.e., a few adsorption sites) was proposed.[10] The current theoretical study now intends to elucidate the electronic mechanisms involved in catalytic promotion, which requires detailed knowledge on structural properties of the CeO_x/Pt(111) interface.

Apart from Pt(111),[9–16] cerium or ceria were deposited onto single crystals of Au(111),[17] Cu(111),[18–20] Ni(111),[21] Pd(111),[22] Rh(111),[23] and Ru(0001).[21,24] Surface-structure-resolving techniques such as scanning-tunneling microscopy (STM) and low-energy electron diffraction (LEED) reveal that ultrathin ceria layers expose the energetically most stable (111)-oriented surface while preserving the bulk fluorite-type structure on the (111)-oriented surfaces of Cu,[18–20] Ni,[21] Pd,[22] or Pt;[11–15] despite the formation of defects and oxygen vacancies typical for ceria surfaces,[25–27] which are topics that are not considered in this study.

STM measurements showed that adsorption of ceria in the submonolayer regime yielded small ceria islands with a height resembling a monolayer (ML) thickness (∼0.3 nm), i.e., a O-Ce-O trilayer.[10,15] Even homogeneous films of ML thickness have been observed by choosing proper preparation.[20] LEED measurements revealed the formation of a periodic (1.4 × 1.4) superstructure on Rh(111)[23] and Pt(111),[12,14] whereas on Cu(111), a (1.5 × 1.5) superstructure was found.[20] All the experimentally observed structures were rotationally aligned with respect to the crystallographic axes of the substrate. The fractional number of 1.4, using Wood's notation, is slightly larger than the real ratio (1.37) of the lattice spacings of (111)-terminated ceria ($a = 3.83$ Å) and Pt(111) ($a = 2.80$ Å). A slight expansion of the ceria adlayer allows 5 ceria lattice constants matching 7 Pt constants and thus the (1.4 × 1.4) superstructure represents a 5 : 7 matching of the lattices. For Cu(111) the observed (1.5 × 1.5) pattern therefore corresponds to a 2 : 3 lattice matching. Another study by Hardacre *et al.*[11] also reported a (4 × 4) LEED pattern when oxidizing cerium to ceria on Pt(111). This pattern corresponds to a somewhat simpler 3 : 4 lattice matching (or a lattice constant ratio of 1.33). Since the ratio of the two bulk lattice constants (1.37) does not result in a commensurate superstructure, we

decided to investigate herein both lattice-constant ratios of 1.4 and 1.33 using a monolayer coverage of ceria, based on the experimental findings mentioned above. Below, we refer to the (4×4) and (1.4×1.4) structures as 3 : 4 and 5 : 7, respectively, because in our opinion this terminology describes the lattice matching more precisely, as discussed in more detail in Sec. III.

However, the exact adsorption geometry, i.e., the atom-to-atom matching of ceria on Pt(111), could not be deduced from experimental studies so far, despite numerous efforts. Although systems involving ceria and platinum have already been investigated using theoretical methods, to our knowledge no computational study has yet been undertaken on the experimentally observed structures; Alfredsson and Catlow[28] examined single layers of Pt and Pd on top of $CeO_2(111)$ and $ZrO_2(111)$ surfaces but they used a 1 : 1 matching of the lattice constants of oxide and metal. Yang *et al.*[29] investigated systems where a single Pt atom is deposited on top of a $CeO_2(111)$ surface. Similar studies were reported by Yang *et al.*[30] and Wilson *et al.*[31] on $Pd/CeO_2(111)$ and by Lu and Yang on various noble-metal clusters adsorbed on $CeO_2(111)$.[32] In addition, calculations were performed dealing with the adsorption behavior of CO on ceria-supported Pt clusters.[33,34] Thus, there is an obvious need in computational studies of ceria monolayers on fcc surfaces such as Pt(111).

II. COMPUTATIONAL DETAILS

All calculations of this contribution were performed using the WIEN2K software package.[35] This DFT-based software has implemented the full-potential APW+lo/LAPW+LO method[36,37] and offers the possibility to explore many different exchange-correlation potentials.[38] The plane-wave cut-off, defined by the product of the smallest atomic-sphere radius times the magnitude of the largest reciprocal lattice vector $R_{\mathrm{MT_{min}}} K_{\mathrm{max}}$, was set to 5.0 in all cases and a G_{MAX} (magnitude of largest vector in the charge-density Fourier expansion) of 12 bohr^{-1} was used for all calculations. 1500 (4685) local orbitals were added for an accurate description of lower-lying s, p, and d semicore states of the 3 : 4 (5 : 7) structure. The Pt $5p$, $5d$, and $6s$, the cerium $5s$, $5p$, $5d$, $4f$, and $6s$, and the oxygen $2s$ and $2p$ states were treated as valence states. The atomic-sphere radii R_{MT} were set to 2.15 bohr (1.14 Å) for Pt, 2.35 bohr (1.24 Å) for Ce, and 1.60 bohr (0.85 Å) for oxygen. The number of k points in the unit cell was 49 $(7 \times 7 \times 1)$ for the 3 : 4 structure and 9 $(3 \times 3 \times 1)$ for the 5 : 7 structure, resulting in 16 and 4 k points in the irreducible Brillouin zone (IBZ), respectively. The Brillouin-zone integration was done using a temperature broadening of 0.068 eV. We used the generalized-gradient approximation (GGA) in the implementation of Perdew, Burke, and Ernzerhof[39] (PBE) to describe electron exchange and correlation and added an effective Hubbard parameter[40,41] $U_{\mathrm{eff}} = U - J$ of 5 eV (using the standard double-counting correction) to account for the strong on-site Coulomb interaction of the Ce $4f$ orbitals. The size of U_{eff} was chosen in accordance with earlier theoretical works by Nolan *et al.*,[42,43] who found that with $U_{\mathrm{eff}} \geqslant 5$ eV the electronic structure of CeO_2 was essentially converged with respect to localization. The geometry optimizations were performed until the forces on all atoms were less than 0.05 eV/Å.

III. GEOMETRICAL DETAILS.

In this study, we calculate the properties of $CeO_2(111)$ layers deposited on a Pt(111) substrate. We investigate both the 3 : 4 and the 5 : 7 superstructures reported in literature and concentrate our efforts on the case of monolayer deposition, leading to a single O-Ce-O trilayer sandwich sitting on top of the Pt(111) surface. This is the thinnest possible ceria layer that is compatible with electrostatics and stoichiometry.

The Pt(111) metal support (substrate) was modeled in all our calculations as a slab which has 5 atomic layers, inversion symmetry, and a lattice constant of 2.80 Å. We set up a 4×4 supercell of this Pt substructure for the 3 : 4 structures and a 7×7 supercell for the 5 : 7 structure. Bulk CeO_2 is an insulating rare-earth oxide that is known to crystallize in the fluorite structure type with an experimental lattice constant a of 5.41 Å.[44] A (111)-oriented surface slab, which is known to be the most stable surface,[45] has a lattice constant of $a/\sqrt{2} = 3.83$ Å. The $CeO_2(111)$ layer was relaxed prior to adsorption under the restriction of fixed cell parameters matching the Pt layer. The ceria lattice constant had to be slightly adapted in both cases to fit this matching, leading to a $\sim$3% contraction with respect to the "bulk" $CeO_2(111)$ lattice constant for the construction of the 3 : 4 structure (giving 3.73 Å) and an $\sim$2% expansion for the construction of the 5 : 7 structure (giving 3.92 Å). The changes of the atomic positions during relaxation were found to be small (i.e., $\leqslant$0.05 Å). The relaxed ceria layers were positioned on both sides of the Pt slab in order to preserve inversion symmetry and matched to the periodicity of the Pt slab (i.e., using a 3×3 ceria supercell for the 3 : 4 structures and a 5×5 ceria supercell for the 5 : 7 structure). The lattice constant of the resulting supercell was fixed for all subsequent calculations. A (pseudo)vacuum layer of 17 Å was added to the combined structure slabs in z direction (i.e., perpendicular to the surface).

To our knowledge the exact matching geometry of ceria on Pt(111) is not known from experiments. Therefore, a large variety of initial adsorption geometries is possible, depending on the lateral positions between surface and adsorbate. Figure 1 displays schematic top views of the (111)-oriented surfaces of CeO_2 [Fig. 1(a)] and platinum [Fig. 1(b)] in the periodicity of the 3 : 4 superstructure. There are three inequivalent atomic species in a free $CeO_2(111)$ surface layer, namely one Ce and two oxygen atoms, of which one is positioned *above* and the other below the plane of cerium atoms. In the following, the oxygen atoms above the Ce plane are named O_s (for surface oxygen) and colored light green, whereas the oxygen atoms below the Ce plane are labeled O_i (for interface oxygen) and colored dark red. After adsorption on the Pt slab, the symmetry of the ceria layer is significantly lowered as indicated by the numbering scheme of the individual atoms in Fig. 1, where the same number is given to equivalent atoms. This scheme is used for identification in the analysis performed in the following sections.

In the case of the 3 : 4 structure, the 3×3 supercell of ceria (slightly adjusted in lattice constant) matches the 4×4 supercell of the Pt substrate, but the lateral position is not yet

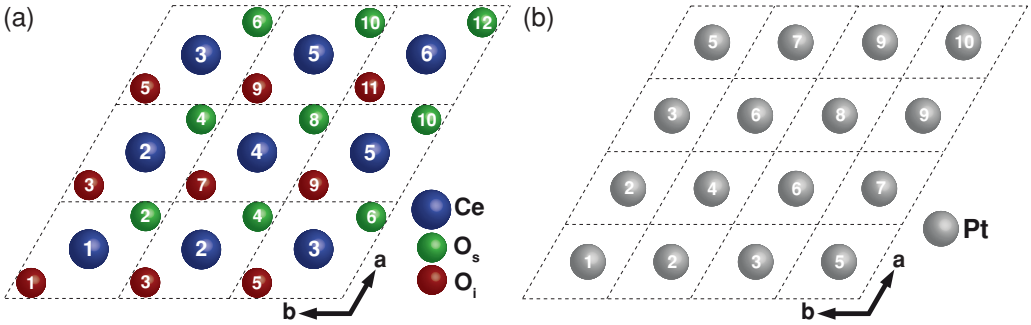

FIG. 1. (Color online) Schematic top views of the (111) surfaces of adsorbate and substrate layers leading to the periodicity of the 3 : 4 structure: (a) 3 × 3 supercell of ceria and (b) 4 × 4 supercell of platinum. In the case of ceria, the positions of the two inequivalent oxygen atoms relative to the cerium atoms are indicated by their color (surface O_s are colored light green, interfacial O_i are colored dark red). The atoms are numbered according to their equivalence in the interface system. The unit cells of the high-symmetry substructures are indicated with dashed lines.

defined. We focused our attention on a matching scenario with one atom being located essentially above another atom. Thus we investigated three different geometries for the matching between substrate and adsorbate in case of the 3 : 4 structure. We chose a geometry where (i) the Ce atom Ce6 [in Fig. 1(a)] is on top of Pt10 [in Fig. 1(b)], termed Ce type, (ii) the interfacial O_i oxygen atom O_i1 (actually the periodic image next to O_s12) is positioned on the same Pt10 atom, a geometry named O_i type, and (iii) the surface oxygen O_s12 is on top of Pt10, this geometry was named O_s type. For the 5 : 7 structure type, only one matching geometry was investigated because the sheer size of the supercell already guarantees a large variety of lateral atomic configurations.

IV. RESULTS AND DISCUSSION

A. Adsorption geometries

After the structures were set up as described in Sec. III, an optimization of the atomic positions was performed for each structure under the restriction of a fixed cell volume. The relaxed structures are shown in Fig. 2 for both substrate to adsorbate ratios. Relaxation resulted in a significant corrugation of both, the Pt interface layer and the ceria adlayer. The displacements of the atoms in the z direction are listed in Table I (in case of the 5 : 7 structure, only the largest movements for each atomic species are listed). The lateral positions between substrate and adlayer atoms (relative to each other) also changed depending on the starting geometry; for example, the oxygen atom O_s12, which initially was positioned on top of Pt10 in the O_s-type geometry, moved away from this position towards Pt8. In contrast, Ce6 in the Ce-type and O_i1 in the O_i-type structure retained their original location with respect to the underlying Pt layer.

The corrugation of the surface Pt layer (difference between the highest and lowest surface Pt atom) amounts to a value between ∼0.3 Å (O_i type) and ∼0.5 Å (5 : 7). The highest interface Pt atoms were found in all structures to be those with an O_i-type oxygen in (or near) an on-top position. In case of the 3 : 4 structures, this is evident in the following examples (cf. Table I): (i) in the Ce geometry Pt1 and Pt2 are the highest platinum atoms (+0.22 and +0.21 Å) and have O_i1 and O_i3 on top, (ii) in the O_i geometry Pt10 lies high (+0.22 Å) and has O_i1 on top, (iii) in the O_s geometry Pt8 has O_i11 on top and thus lies high (+0.26 Å), showing the maximum upward movement of all 3 : 4 structures with respect to a free-standing Pt layer.

The Pt atoms, which show the largest downward corrugation (up to −0.16 Å in the direction of the bulk), are always those with an O_s atom above them. For example, Pt6 and Pt8 with O_s4 and O_s8 above in case of the Ce structure, Pt1 with O_s2 above for the O_i type, and also Pt1 with O_s2 above in case of the O_s geometry.

The corrugation of the cerium atoms was found to be even bigger where the difference between the highest and lowest Ce atom was ∼0.5 Å in both the O_i and 5 : 7 structures, ∼0.6 Å in case of the O_s structure, and even 0.8 Å for the Ce geometry. In general, the Ce atoms follow the trend of the Pt atoms; in any case those Ce atoms that moved away from the interface the most, are situated above the highest-lying Pt atoms: Ce1 above Pt1/Pt2 for the Ce geometry, the Ce1/Ce3 triangle above Pt10 for O_i, and the Ce5/Ce6 triangle above Pt8 for the O_s type, all showing an ∼+0.3 Å upward movement compared to the average position of all cerium atoms. The same trend can also be observed in the opposite direction: Ce4 (for Ce), the Ce2/Ce4 triangle (for O_i), and the Ce1/Ce3 triangle (for O_s) are the lowest-lying Ce atoms, all of which are situated in the vicinity of the lowest Pt atoms.

For the oxygen atoms the interpretation of the relative movements is not as clear: the highest-positioned interface oxygen atoms are O_i5/O_i11 for Ce, O_i11 for O_i, and O_i7 for O_s type. The highest surface oxygen atoms are positioned around the highest Pt atoms: O_s2/O_s6 around Pt1 and Pt2 for Ce, O_s6 and O_s12 around Pt10 for O_i, and O_s8/O_s10 around Pt8 for O_s type. In each case, the lowest interface oxygen atoms are situated near the lowest Ce atoms: the O_i7 and O_i9 triangle around Ce4 for the Ce type, $O_i3/O_i5/O_i7/O_i9$ around Ce2/Ce4 for O_i, and $O_i1/O_i3/O_i5/O_i9$ around Ce1/Ce3 for O_s. Finally, the lowest-lying surface oxygen atoms are the O_s4/O_s8 triangle for the Ce-type geometry, situated around Ce4, the lowest cerium atom in this particular geometry, $O_s2/O_s4/O_s8/O_s10$ around Ce2/Ce4 for O_i, and $O_s2/O_s4/O_s6/O_s12$ around Ce1/Ce3 for O_s, thus following (like the cerium atoms) the trend of the underlying Pt atoms.

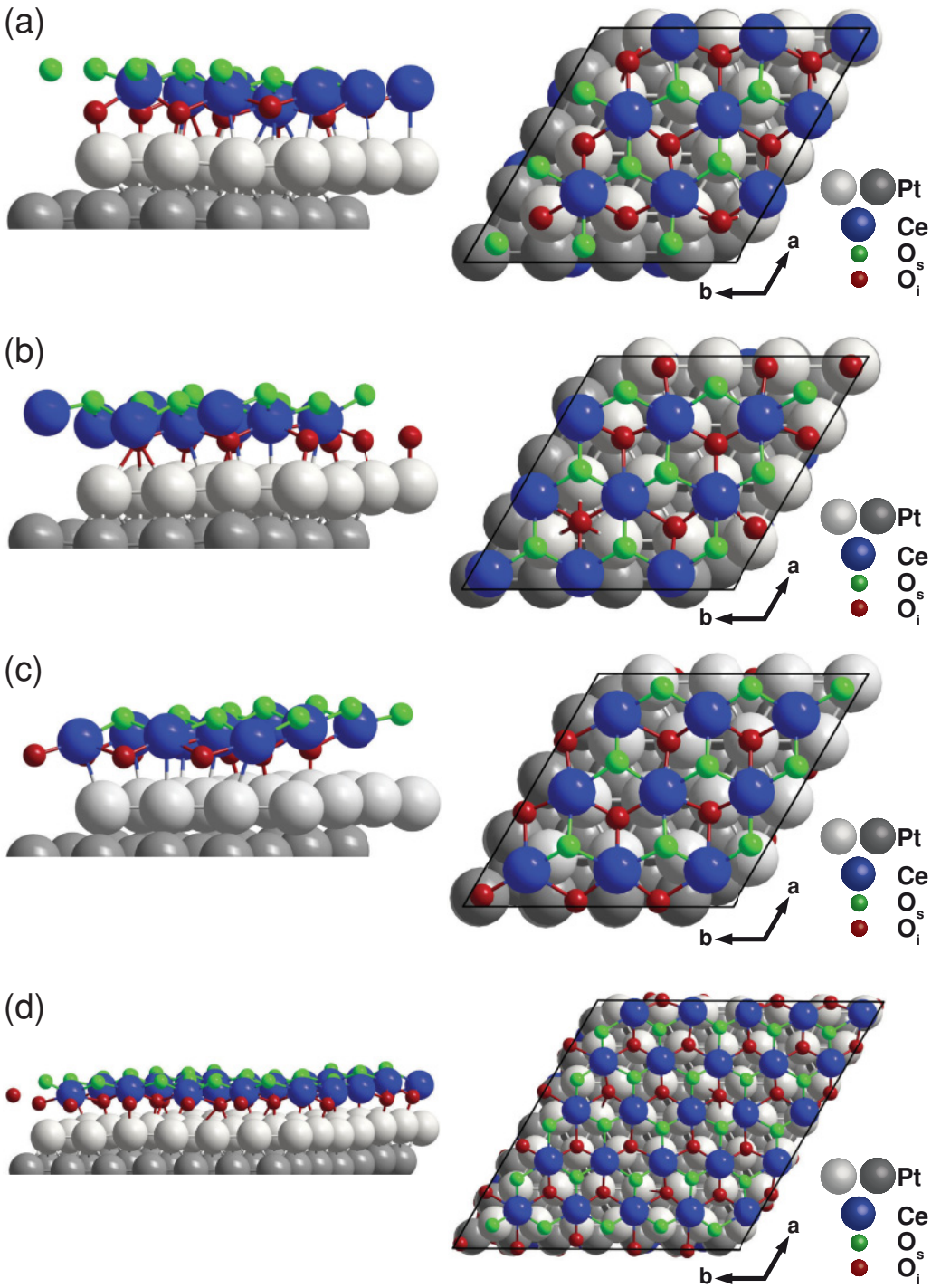

FIG. 2. (Color online) Ball models of the different 3 : 4 and 5 : 7 structure types after geometry optimization: (a) Ce, (b) O_i, (c) O_s, and (d) 5 : 7 type. Left panels show a side view along the short diagonal of the unit cell, right panels a top view. The original matching was done in all cases by positioning a Ce, O_s, or O_i atom on top of the Pt atom in the upper right corner of the supercell. To improve the visibility of the Pt surface layer, the interface Pt atoms are plotted in light grey and the subsurface Pt atoms appear in a darker shade.

For all calculated geometries the described surface buckling resulted in changes with respect to the corresponding Pt-Pt and Ce-O bond lengths. While the Pt-Pt bond lengths on average remained constant (compared to the value of 2.80 Å of bulk Pt), individual changes were as large as ±0.05 Å with reduced (enhanced) bond lengths between the lowest (highest) situated Pt atoms and their respective nearest neighbors. The Ce-O bond lengths showed larger deviations of up to ±0.15 Å from the value of 2.33 Å (3 : 4) or 2.40 Å (5 : 7) of a free-standing CeO_2 layer relaxed in the corresponding unit cell.

In conclusion of this analysis, one can state that the corrugation of the ceria adsorbate layer follows, in principle, simple trends: interface oxygen atoms in (or near) an on-top Pt position cause an upward movement of the corresponding

TABLE I. Corrugation of the Pt interface and the ceria adsorbate layer after relaxation in the assumed structures. Movements of the atoms in z direction are given in Å relative to a relaxed free-standing slab (in case of platinum atoms) or average positions (in case of cerium and oxygen atoms). For the 3 : 4 geometry the movements of all atoms in the three types Ce, O_i, and O_s are listed. For the 5 : 7 geometry only the maximum movements of the respective atomic species are included.

Atom	Ce (Å)	O_i (Å)	O_s (Å)	5 : 7 (Å)	Atom	Ce (Å)	O_i (Å)	O_s (Å)	5 : 7 (Å)
Pt1	+0.22	−0.09	−0.10		O_i1	−0.01	+0.07	−0.04	
Pt2	+0.21	−0.06	−0.06		O_i3	−0.03	−0.11	−0.09	
Pt3	+0.02	+0.11	−0.06		O_i5	+0.21	−0.10	−0.09	+0.50/−0.20
Pt4	+0.10	−0.06	−0.02		O_i7	−0.20	−0.07	+0.28	
Pt5	+0.03	+0.09	−0.08	+0.29/−0.16	O_i9	−0.20	−0.11	−0.07	
Pt6	−0.11	−0.03	+0.15		O_i11	+0.22	+0.33	+0.11	
Pt7	+0.09	−0.07	+0.13		O_s2	+0.12	−0.09	−0.15	
Pt8	−0.14	−0.03	+0.26		O_s4	−0.23	−0.11	−0.13	
Pt9	−0.01	+0.13	+0.15		O_s6	+0.14	+0.23	−0.10	+0.38/−0.23
Pt10	±0.00	+0.22	−0.07		O_s8	−0.24	−0.14	+0.25	
Ce1	+0.31	+0.28	−0.26		O_s10	+0.09	−0.13	+0.23	
Ce2	−0.02	−0.24	−0.05		O_s12	+0.12	+0.23	−0.10	
Ce3	+0.02	+0.27	−0.25	+0.31/−0.23					
Ce4	−0.46	−0.24	−0.02						
Ce5	−0.01	−0.03	+0.28						
Ce6	+0.16	−0.03	+0.29						

interface Pt atom and a reduced Pt-O distance. In turn, surface oxygen atoms in an on-top position make the interface Pt atoms move toward the bulk.

B. Energetics

In order to identify the most stable adsorption geometry among the calculated structures we compared their total energies, which are listed in Table II. The numbers indicate that the O_s-type geometry is the most stable among the 3 : 4 structures investigated. For an explanation, one can apply a simple model based on the results of Yang *et al.*[29] and Mayernick *et al.*[46] comparing the various possible adsorption sites of single Pt or Pd atoms on the CeO_2(111) surface based on their respective adsorption energies; the results indicate that the most favorable position for a Pt atom is on top of or near an oxygen atom that is positioned away from the metal/oxide interface. In our case, this would correspond to an O_s-type oxygen atom. However, the most unfavorable position for a Pt atom was found to be on top of a Ce atom. Applying this simple model to the three investigated 3 : 4-type geometries (see Fig. 2), one realizes that the relaxed Ce-type geometry still contains a Ce atom (namely, Ce6) on top of a Pt atom (Pt10), leading to reduced stability. This feature is absent in both other geometries O_i and O_s, which, in addition, have a more favorable match of the O_s oxygen atoms with the surface Pt layer, making these geometries more stable.

TABLE II. Total energies E_{tot} and adsorption energies E_{ads} of the 3 : 4 and 5 : 7 geometries investigated. Total energies are given in eV relative to −44 572 770 eV (3 : 4) and −135 246 955 eV (5 : 7). Adsorption energies are given in eV per formula unit CeO_2.

Geometry	E_{tot} (eV)	E_{ads} (eV/formula unit)
Ce-type	−0.8301	−0.50
O_i-type	−0.8989	−0.50
O_s-type	−1.1150	−0.52
5 : 7	−0.2501	−0.83

For each geometry we also calculated the adsorption energies of the adsorbate layers. The adsorption energy E_{ads} of the ceria layer was obtained by using the following equation:

$$E_{ads} = \tfrac{1}{2}(E_{tot} - E_{CeO_2} - E_{Pt}), \quad (1)$$

where E_{tot} is the total energy of the relaxed adsorption geometry, E_{CeO_2} is the total energy of two unadsorbed ceria layers after relaxation, and E_{Pt} is the total energy of a free-standing Pt slab without adsorbates that was relaxed in the same unit cell. Finally, the prefactor of 1/2 accounts for the presence of two ceria adsorbate layers on both sides of the slab. A negative value of the resulting adsorption energy corresponds to a stabilizing interaction between metal surface and adsorbate layer and thus the lowest obtained number represents the most stable adsorption geometry. Table II gives the calculated adsorption energies per formula unit CeO_2. Although the differences are rather small, the O_s geometry still shows the highest adsorption energy (−0.52 eV) among the 3 : 4 structures, a result which corroborates that this structure is indeed the most stable, at least among those investigated. The adsorption energy for the 5 : 7 structure is slightly higher (−0.83 eV), which is also consistent with the fact that in this geometry the mean distance between the layers of surface Pt and Ce atoms is smaller (decrease by ∼0.15 Å) compared to the 3 : 4 types. This may be due to the fact that the CeO_2 lattice constant is contracted in case of the 3 : 4 structure and expanded for the 5 : 7 structure (as compared to bulk ceria). Therefore, also

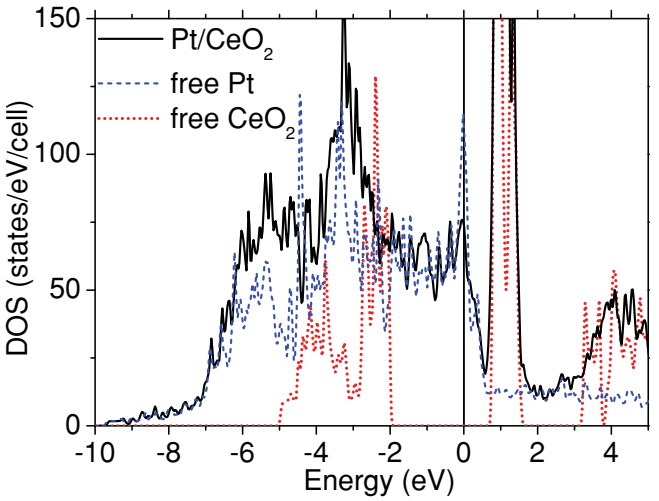

FIG. 3. (Color online) Total density of states (TDOS) of CeO_2/Pt (solid black line), a free Pt slab (dashed blue line), and unadsorbed CeO_2 (dotted red line) for the 3 : 4 (O_s type) structure (values are given in states/eV/cell). The Fermi energy ε_F is marked with a line. Energies are given in eV relative to ε_F. The DOS of unadsorbed CeO_2 is down-shifted by 0.65 eV to align the Ce-4*f* peak with the Ce-4*f* peak of the interface system.

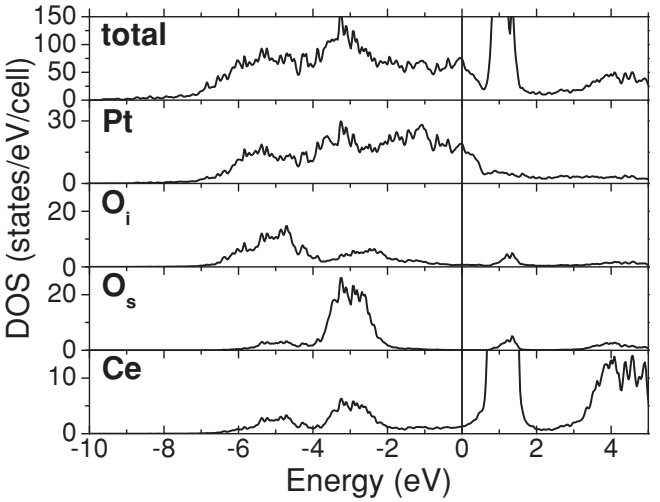

FIG. 4. Total density of states (TDOS) and partial density of states (PDOS) of all atomic species for the 3 : 4 (O_s-type) structure (values are given in states/eV/cell). Only the Pt atoms of the interface layer were included in the respective PDOS. The Fermi energy ε_F is marked with a line. Energies are given in eV relative to ε_F.

the Ce-O bond distances differ between the two matching geometries.

Based on these findings we focus on the most stable O_s-type geometry for all further analyses below, performed for the 3 : 4 geometry.

C. Density of states (DOS)

Since the bonding character between a substrate and an adsorbate directly affects the catalytic behavior of the resulting interface system, special attention was paid to the analysis of the electronic structure. Figure 3 shows the total density of states (TDOS) of three cases: (i) the Pt/CeO_2 system (3 : 4, O_s-type geometry), (ii) a free-standing ceria layer (for which its TDOS has been down-shifted in energy by 0.65 eV to match the Ce-4*f* peak with the Ce-4*f* peak of the interface system), and (iii) an adsorbate-free Pt slab after relaxation. Contrary to the insulating behavior of the free-standing ceria layer, which has a calculated band gap of ∼2.5 eV, the CeO_2/Pt(111) interface system clearly shows a metallic character. This originates from the 5*d* states of the Pt slab, which fall in the gap between the O-2*p* and Ce-4*f* bands. The DOS of the interface system (i) can thus be seen as a superposition of the two free-standing structures of Pt (ii) and ceria (iii). The contribution from the O-2*p* states of free ceria between −2 eV and −5 eV is now visible between −4 eV and −7 eV in the interface system. The Pt bandwidth is hardly modified upon forming the interface, whereas the O-2*p* band of CeO_2 becomes much wider and thus the interface DOS (i) is much larger than the superposition (ii) + (iii) in this energy range, indicating that some O-2*p* states must have been shifted downward.

To further elucidate the electronic structure, the partial densities of states (PDOS) of all atomic species are shown in Fig. 4 for the 3 : 4 geometry (for the Pt atoms only the surface layer has been considered). The DOS of the 5 : 7 geometry is very similar and thus is not shown here but the following analysis applies to both interface structures.

The cerium PDOS consists of low lying 5*s* bands at ∼−35 eV, 5*p* bands at ∼−20 eV, and 5*d* states in the valence-band region as minor contributions. It is mostly dominated by the 4 *f*states below and above the Fermi level with a small bonding and a large antibonding contribution. The platinum PDOS is dominated by broad peaks around the Fermi level, which have 5*d* character. The oxygen DOS consists of low-lying 2*s* states at ∼−20 eV, bonding 2*p* states just below the Fermi level and antibonding 2*p* states at ∼+1.3 eV that interact with the Ce-4*f* and 5*d* states. One striking feature is a remarkable difference between O_i and O_s oxygen; the O_i PDOS shows two peaks at about −5 and −2.5 eV whereas O_s has only one at about −3 eV. Ce-4*f*, Ce-5*d*, and some Pt-5*d* states contribute to all these oxygen peaks below ε_F, indicating interactions between the oxide layer and the metal surface. Figure 5 shows two contrasting examples of this interaction depending on the individual matching geometry: the top panel shows the PDOS of the $5d_{z^2}$ orbital of Pt8 and the $2p_z$ orbital of O_i11, which are situated on top of each other as can be seen in Fig. 2(c) when looking at the labels in Fig. 1. The Pt d_{z^2} orbital is split in energy with characteristic bonding peaks at ∼−6 eV and ∼−3.3 eV, which show a strong overlap with the p_z orbital of O_i11. Besides that a nonbonding contribution at ε_F and an antibonding interaction with O_i11 at ∼ +1.3 eV are also evident. In contrast, the bottom panel of Fig 5 shows an example of a weak interaction between substrate and adsorbate, namely the PDOS of the $5d_{z^2}$ orbital of Pt10 and the $2p_z$ orbital of O_i1. Because these atoms do not nearly have the same matching as the above example [O_i1 is more in a threefold hollow position above Pt5/Pt10, as can be seen in Fig. 2(c)], the overlap between the displayed orbitals is rather poor.

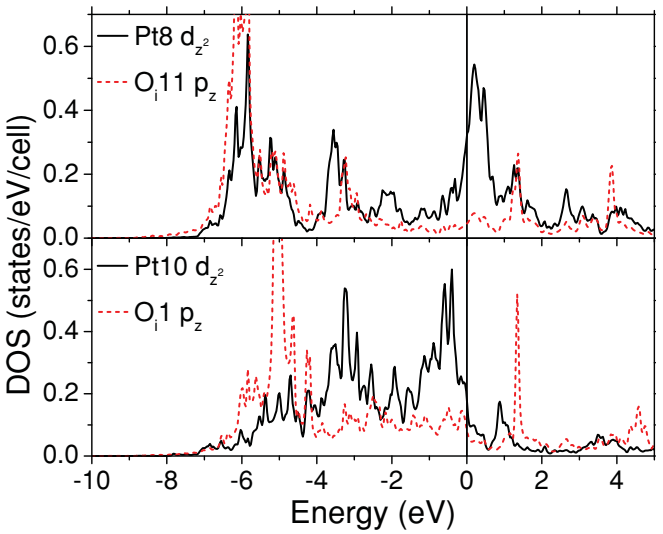

FIG. 5. (Color online) Two PDOS plots for the 3 : 4 (O_s-type) structure illustrating the differences in interaction between substrate and adsorbate layer. Upper panel: PDOS of Pt8 ($5d_{z^2}$ orbital, solid black line) and O_i11 ($2p_z$ orbital, dashed red line) as an example of a strong interaction between interface oxygen and platinum. Lower panel: PDOS of Pt10 ($5d_{z^2}$ orbital, solid black line) and O_i1 ($2p_z$ orbital, dashed red line), which do not match well geometrically. Values are given in states/eV/cell. The Fermi energy ε_F is marked with a line. Energies are given in eV relative to ε_F.

D. Electron density and bonding character

To further analyze the bonding character of the various structures their electron densities were investigated. We focus on the 3 : 4 structure, since the 5 : 7 structure behaves rather similar, and consider just the valence states in the energy range of −9.5 eV and ε_F. Figure 6 shows the difference electron density (crystalline minus superposed atomic densities) in the $(11\bar{2}0)$ plane (i.e., the plane in the longer diagonal of the supercell). One can clearly see the relaxed CeO_2 layer (with O_s, O_i, and Ce atoms) on top of the Pt atoms, which strongly differ in the electron density according to their environment. We observe a significant polarization of those Pt atoms which have an oxygen sitting on top with a strong electrostatic field (i.e., Pt8 and O_i11 in Figs. 1 and 6). Such a feature is absent for the other Pt atoms shown in the figure. The $5d_{z^2}$ orbital of Pt11 is visible in the electron-density map, showing an electron deficiency compared to the atomic density. On the other hand, there is an increase in the $5d_{xz}$ and $5d_{yz}$ orbitals of the same Pt atom, which can be interpreted as backdonation from O_i11 to the Pt8 5*d* states. This is corroborated by the negative density visible on O_i11 in the direction of the Pt-O bond. Such kind of strong interaction between Pt and oxygen was already seen in the DOS plots (see Sec. IV C and Figs. 4 and 5).

In the CeO_2 layer, a significant polarization of the Ce electron densities in the Ce-O bond direction is visible. The O_s and O_i oxygen atoms differ strongly in their electron-density distribution, a feature which was already observed in the PDOS plots in Fig. 4: all the O_s-type oxygen atoms have a rather similar electron-density distribution with the lone electron pair pointing toward vacuum (having only one peak in the PDOS), whereas the electron density of the O_i-type atoms strongly depends on the chemical environment. This becomes evident from the orientation of the lone pair for O_i11 (pointing toward vacuum) compared to, e.g., O_i1 and O_i7 (pointing toward the interface).

To compare the relaxed structures with STM experiments we calculated the (constant-height) local density of states (LDOS) for the 5 : 7 structure in a plane above the sample surface (see Fig. 7). For this we considered filled states in the energy range $[\varepsilon_F - 3.2\,\text{eV}, \varepsilon_F]$, in agreement with typical sample bias voltages used in STM experiments.[14,15] The distance between the chosen plane and the topmost O_s atom of the surface was found to be very crucial for the appearance of the resulting LDOS plots; if the distance is $\geqslant$5.7 Å, an almost featureless electron density is obtained, which does not provide any information about the positions of the surface atoms. This observation is, in principle, comparable to the experimental difficulties in obtaining an STM image of ceria surfaces with atomic resolution because typical working distances between the STM tip and the sample surface are in the range of 5–10 Å. On the other hand, calculating the LDOS in a plane very close to the topmost O_s atom (∼2 Å) yields an electron density that is mostly dominated by the 2*p* states of the O_s atoms.

For the LDOS plot in Fig. 7, we, therefore, opted for an intermediate distance of 3.6 Å, where filled states from the surface O_s atoms but also contributions from Ce and O_i atoms are visible. As discussed in Sec. IV A, the very bright spots indicate O_s atoms with the largest outward relaxation, while

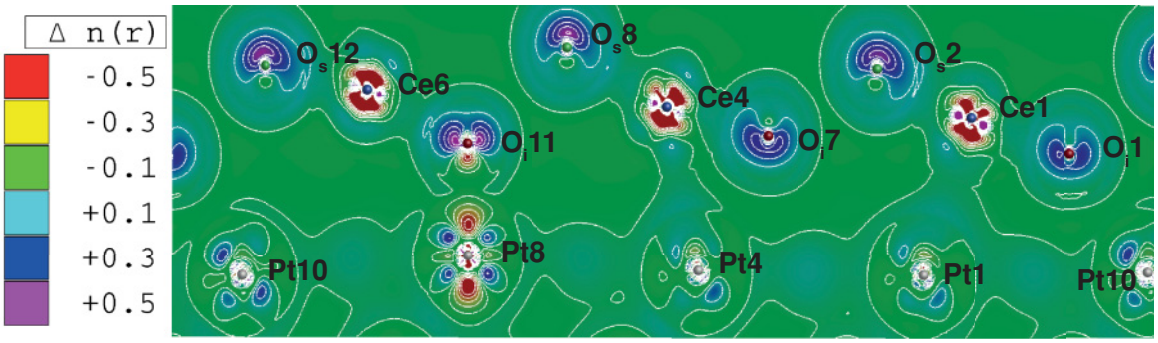

FIG. 6. (Color online) Difference electron density $\Delta n(r)$ in the $(11\bar{2}0)$ plane of the 3 : 4 (O_s-type) structure taken for the valence states that lie between −0.7 Ry (−9.5 eV) and ε_F. The positions and labels of the atoms correspond to Fig. 1, going from the top right (Pt10) via Pt8 and Pt4 to the bottom left (Pt1). The electron density is given in e/Å^3. Electron excess is marked with pink, electron deficiency with red color, and green color marks areas with electron-density differences close to zero. The graph was produced using XCRYSDEN.[47]

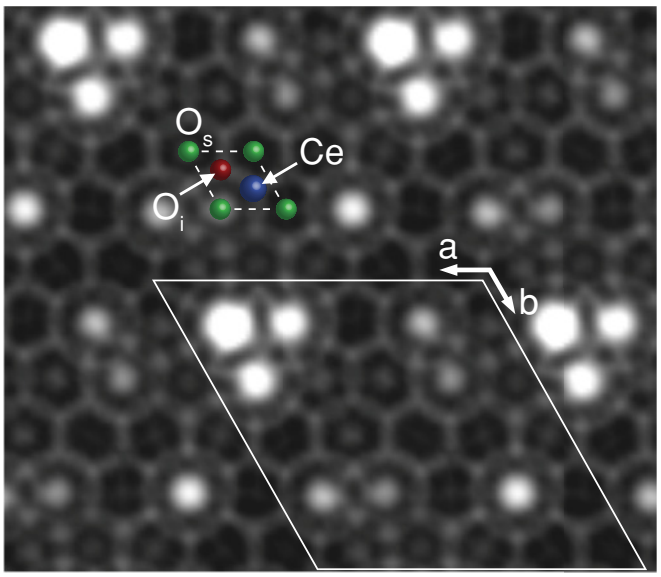

FIG. 7. (Color online) Constant-height local-density-of-states (LDOS) plot of a 2×2 supercell of the 5 : 7 structure. The plot shows filled states in the energy range $[\varepsilon_F - 3.2\,\text{eV}, \varepsilon_F]$ in a plane 3.6 Å above the topmost O_s oxygen atom. The unit cell of the 5 : 7 structure (solid lines, see Fig. 2 for details) and a high-symmetry CeO_2 unit cell (dashed lines) are indicated in the plot. The positions of the individual atoms are denoted by colored spheres.

some fairly dark areas correspond to O_s atoms with inward relaxation. In addition, the Ce and O_i atoms are visible as gray spots. Their intensity increases relative to the bright O_s spots when the surface-tip distance is increased.

Unfortunately, the comparability of the LDOS plots to experimental results is rather limited. The superstructure due to the CeO_2/Pt lattice mismatch has not be seen yet, probably because the experimentally observed ceria films[15] are defect rich with features such as oxygen vacancies, adsorbed water, hydroxyl groups, etc. As already mentioned, all these properties were not considered in this study.

To obtain a deeper understanding of the changes in the electronic distribution that occur upon adsorption, we analyzed the charges on the atoms using the atoms-in-molecules[48] (AIM) method. This scheme analyzes the topology of the charge density. It divides space into atomic volumes (basins) containing exactly one nucleus based on the definition of an interatomic surface that satisfies the zero-flux boundary condition

$$\nabla\rho(\mathbf{r_S})\mathbf{n}(\mathbf{r_S}) = 0, \tag{2}$$

where $\mathbf{n}(\mathbf{r_S})$ is the unit vector normal to the surface and $\nabla\rho(\mathbf{r_S})$ is the gradient of the electron density at $\mathbf{r_s}$. This decomposition is uniquely defined and thus considerably improves comparability between different calculations since it is independent of the basis set.

We compared the AIM charges of the atoms before and after adsorption of the ceria adlayer for both structure types. Subtraction of these values allows estimating the charge transfer due to adsorption. In Table III the results of this analysis are listed for the 3 : 4 (O_s-type) structure. Note that we have only considered the Pt atoms of the topmost (i.e., surface) layer of the slab for this analysis.

All cerium atoms gain electrons during adsorption and show a decrease of positive charge between 0.03 and 0.15e for the 3 : 4 and between 0.03 and 0.17e for the 5 : 7 structure. The gain of electrons is higher on those cerium atoms that have moved closer to the interface during relaxation (see Sec. IV A for details), i.e., Ce1 and Ce3 in the O_s-type structure. The charge of the oxygen atoms in the surface O_s position [even numbers in Fig. 1(a) and Table III] is almost unperturbed — at most a very small transfer of electrons of $\pm 0.01e$ is observed for the 3 : 4 and $\pm 0.02e$ for the 5 : 7 structure. In contrast, all interface O_i oxygen atoms [odd numbers in Fig. 1(a) and Table III] lose a small fraction of electrons in both geometries, namely, between 0.05 and 0.09e (3 : 4) and 0.04–0.12e (5 : 7). This loss can be attributed to the aforementioned backdonation of electrons from the oxygen to some of the Pt atoms, which was also visible for O_i11/Pt8 in the electron density map in Fig. 6. All Pt atoms of the 3 : 4 geometry that have moved toward the ceria adlayer during relaxation (for details see Sec. IV A), namely, Pt6 to Pt9, lose a significant fraction of electrons (0.24–0.26e) whereas the ones which moved farther away from the interface (Pt1 to Pt5 and Pt10) show a slightly increased number of electrons (0.06–0.13e). The same is true for the 5 : 7 structure with an electron increase of 0.05–0.18e for the Pt atoms corrugated toward the ceria layer and an electron decrease of 0.09–0.25e for the Pt atoms corrugated away. The loss of electrons of the Pt atoms close to the interface is in qualitative accordance with results from literature on a NM/CeO_2 system (NM = Pt and Pd), for which an overall electron transfer from the noble metal atoms to the Ce^{4+} surface ions was observed.[31,32] This electron transfer causes an increase of Ce^{3+} ions on the catalyst surface, thus significantly altering the catalytic activity of the system.

A useful tool to interpret the character of the individual chemical bonds is the analysis of the metallicity/ionicity at the bond critical points (BCPs) that were obtained with AIM. For this purpose we calculated three measures of bond metallicity (proposed in Refs. 49,50), namely the values of ξ_j and ξ_m, as well as Bohm's quantum potential W_{GEA}, for all atoms of the 3 : 4 (O_s-type) geometry. These quantities are defined

$$\xi_j(\mathbf{r}_{\text{bcp}}) = \frac{\rho(\mathbf{r}_{\text{bcp}})}{\nabla^2\rho(\mathbf{r}_{\text{bcp}})} \text{ for } \nabla^2\rho(\mathbf{r}_{\text{bcp}}) > 0, \tag{3}$$

$$\xi_m(\mathbf{r}_{\text{bcp}}) = \frac{36(3\pi^2)^{\frac{2}{3}}}{5}\frac{(\rho(\mathbf{r}_{\text{bcp}}))^{\frac{5}{3}}}{\nabla^2\rho(\mathbf{r}_{\text{bcp}})} \text{ for } \nabla^2\rho(\mathbf{r}_{\text{bcp}}) > 0, \tag{4}$$

$$W_{\text{GEA}}(\mathbf{r}_{\text{bcp}}) = \frac{5}{36}[\xi_j(\mathbf{r}_{\text{bcp}})]^{-1} - \frac{1}{5}[3\pi^2\rho(\mathbf{r}_{\text{bcp}})]^{\frac{2}{3}}, \tag{5}$$

where $\rho(\mathbf{r}_{\text{bcp}})$ and $\nabla^2\rho(\mathbf{r}_{\text{bcp}})$ are the electron density and the Laplacian at the bond critical point $\mathbf{r}_{\text{bcp}}$, respectively. According to the cited studies, values of $\xi_j(\mathbf{r}_{\text{bcp}}) > 1$, $\xi_m(\mathbf{r}_{\text{bcp}}) > 10$, and $W_{\text{GEA}}(\mathbf{r}_{\text{bcp}}) < 0$ indicate metallic interaction in the case of compounds.

As expected, the bonds between the surface Pt atoms have metallic character with an average value for $\xi_j(\mathbf{r}_{\text{bcp}}) \approx 1.2$, $\xi_m(\mathbf{r}_{\text{bcp}}) \approx 12.5$, and $W_{\text{GEA}}(\mathbf{r}_{\text{bcp}}) \approx -0.17$. The metallicity of these surface Pt-Pt bonds is slightly increased compared to the bonds between the subsurface Pt atoms, which have aver-

TABLE III. Atomic charges and resulting charge transfer compared to the free substructures of Pt and CeO_2 obtained with AIM for the 3 : 4 (O_s-type) CeO_2/Pt(111) structure.

Atom	CeO_2/Pt(111)	free substructure	Charge transfer	Atom	CeO_2/Pt(111)	free substructure	Charge transfer
Pt1	−0.178	−0.047	−0.131	O_i1	−1.182	−1.271	+0.089
Pt2	−0.168	−0.047	−0.121	O_i3	−1.215	−1.272	+0.056
Pt3	−0.176	−0.047	−0.129	O_i5	−1.212	−1.272	+0.060
Pt4	−0.158	−0.047	−0.110	O_i7	−1.213	−1.272	+0.059
Pt5	−0.109	−0.047	−0.061	O_i9	−1.215	−1.271	+0.055
Pt6	+0.192	−0.047	+0.239	O_i11	−1.220	−1.272	+0.052
Pt7	+0.191	−0.047	+0.238	O_s2	−1.264	−1.271	+0.007
Pt8	+0.207	−0.047	+0.255	O_s4	−1.261	−1.272	+0.011
Pt9	+0.197	−0.047	+0.244	O_s6	−1.271	−1.271	±0.000
Pt10	−0.106	−0.047	−0.058	O_s8	−1.285	−1.272	−0.013
Ce1	+2.402	+2.545	−0.142	O_s10	−1.285	−1.271	−0.014
Ce2	+2.468	+2.544	−0.076	O_s12	−1.271	−1.271	±0.000
Ce3	+2.390	+2.544	−0.154				
Ce4	+2.466	+2.544	−0.078				
Ce5	+2.515	+2.545	−0.030				
Ce6	+2.517	+2.544	−0.027				

age values of $\xi_j(\mathbf{r}_{\rm bcp}) \approx 1$, $\xi_m(\mathbf{r}_{\rm bcp}) \approx 10$, and $W_{\rm GEA}(\mathbf{r}_{\rm bcp}) \approx -0.15$. This is comparable to the average bond metallicity of a free-standing Pt layer without ceria adsorbates.

In agreement with the electron-density analysis, the Pt-O bonds are mainly of ionic character, showing an average $\xi_j(\mathbf{r}_{\rm bcp}) \approx 0.3$, $\xi_m(\mathbf{r}_{\rm bcp}) \approx 3$, and a $W_{\rm GEA}(\mathbf{r}_{\rm bcp}) \approx 0.1$. The values for the Ce-O bonds are somewhere in between these two extremes with an average $\xi_j(\mathbf{r}_{\rm bcp}) \approx 0.5$, $\xi_m(\mathbf{r}_{\rm bcp}) \approx 6$, and $W_{\rm GEA}(\mathbf{r}_{\rm bcp}) \approx 0$. There is no significant difference between O_i- and O_s-type oxygen with regard to these parameters. The obtained numbers indicate that the Ce-O bonds already show some signs of covalency, an observation that was also made in STM measurements on CeO_2/Pt(111).[14]

Another area where significant differences exist between surface and interface oxygen atoms is the position of the O 1*s* core level (a histogram plot of the distribution relative to ε_F is shown in Fig. 8 for the 5:7 structure). The 1*s* binding energies of the O_s-type oxygen atoms are centered around −506.0 (3:4) and −505.6 eV (5:7), respectively, whereas the levels of the O_i-type oxygen atoms are downshifted to −506.8 (3:4) and −506.6 eV (5:7), in agreement with a general loss of electrons observed on these atoms according to the AIM analysis mentioned above. The binding energies of the O_s-type oxygen atoms show a narrow distribution, whereas the differences among the O_i species are much more pronounced, e.g., O_i1 in the 3:4 structure shows the largest electron loss in the AIM analysis upon adsorption (0.089*e*, see Table III), but also has a smaller 1s binding energy (−506.7 eV) than the average. The distance from the surface Pt layer seems to play an even more important role: those O_i-type oxygen atoms, which have moved farthest away during relaxation (see Sec. IV A), have by far the smallest 1*s* binding energy of −505.8 eV, which is already very close to the value of the O_s-type oxygen atoms (in case of the 3:4 O_s structure the corresponding atom is O_i7 with a binding energy of −506.3 eV). This special O_i 1*s* core level is indicated with an arrow and a horizontal pattern in Fig. 8.

It occurs from our analysis that the bonding between the Pt substrate and the oxide is mostly dominated by electrostatic forces with some contributions due to hybridization between the Pt layer and interface oxygen. A significant charge transfer exists between the adsorbate and substrate. From these findings we conclude that there is a strong interaction between Pt and the ceria adsorbate present in this system, which is also found experimentally (see, e.g., Ref. 51) and is related to the strong metal support interaction (SMSI) often observed in metal/oxide catalytic systems.[7,52–54]

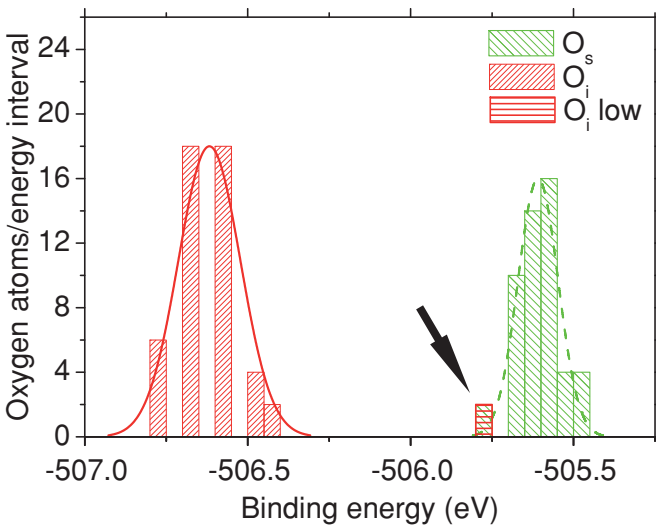

FIG. 8. (Color online) Histogram plot (bin size 0.05 eV) and distribution of the O 1*s* core levels of O_i (solid red line and bars) and O_s (dashed green line and bars) type oxygen atoms in the 5 : 7 structure. The arrow indicates the special O_i-type oxygen atom named O_i low (red horizontal pattern), which has moved far away from the Pt surface and thus has a considerably lower O 1*s* binding energy.

V. SUMMARY

In this paper, DFT calculations on the experimentally reported structures of the CeO_2/Pt(111) interface system are presented. The experimental structures were analyzed by relaxing three different starting geometries in case of the 3 : 4 structure and one in case of the 5 : 7 structure. We investigated the resulting corrugation of the Pt surface and the ceria adlayers, compared the total energies, and calculated the corresponding adsorption energy of the ceria adsorbate for each geometry. The corrugation of the topmost Pt layer in all considered structures followed a systematic pattern where the highest Pt atom always had an interface oxygen atom adsorbed on top. It was found that a simple model based on the stability of different adsorption sites may qualitatively explain the energy differences found in the resulting geometries of the whole interface system. It was also revealed that a direct matching of Ce and Pt is particularly unfavorable for the stability of the interface.

An insight into the electronic properties and the bonding character was achieved by analysis of the density of states and the electron density as well as by investigating the local density of states (LDOS) in a plane above the surface. Strong interactions were detected, which are mainly based on electrostatic interactions between the topmost Pt layer and the oxygen atoms at the interface, but some small contributions from hybridization have been found as well. These results were corroborated by the analysis of the bond metallicity at the bond critical points (BCPs). Upon adsorption, a significant charge transfer occurs between the surface Pt atoms and the cerium and oxygen atoms of the ceria adlayer, depending on the distances between the atoms. The reduction of some of the Ce^{4+} ions seems crucial for the catalytic properties of the system. The position of the O 1*s* core levels is a good measure for the binding situation and depends on the local bonding distances and the charge transfer.

Despite of restricting the structure models to an idealized situation, which ignores topics such as nonstoichiometry, vacancies, stepped surfaces, formation of islands, etc., the present calculations have shown a rich variety of bonding situations with varying bond lengths and charges depending on the local geometry. This provides a new insight into the structure-property relations that are relevant for ceria-based catalysis.

ACKNOWLEDGMENTS

Ch. S., Y. S. and G. R. acknowledge support by the Austrian Science Fund (SFB F45, FOXSI), P. B. was supported by the Austrian Science Fund (SFB F41, ViCoM).

[1] A. Trovarelli, Catal. Rev. Sci. Eng. **38**, 439 (1996).
[2] V. P. Zhdanov and B. Kasemo, Appl. Surf. Sci. **135**, 297 (1998).
[3] A. Törncrona, M. Skoglundh, P. Thormählen, E. Fridell, and E. Jobson, Appl. Catal., B **14**, 131 (1997).
[4] T. Bunluesin, R. J. Gorte, and G. W. Graham, Appl. Catal., B **15**, 107 (1998).
[5] L. P. Bevy, *Frontiers in Catalysis Research* (Nova Science, New York, 2006).
[6] A. F. Carley, *Surface Chemistry and Catalysis* (Kluwer Academic/Plenum, New York, 2002).
[7] K. Hayek, M. Fuchs, B. Klötzer, W. Reichl, and G. Rupprechter, Top. Catal. **13**, 55 (2000).
[8] F. P. Leisenberger, S. Surnev, G. Koller, M. G. Ramsey, and F. P. Netzer, Surf. Sci. **444**, 211 (2000).
[9] Y. Suchorski, R. Wrobel, S. Becker, B. Strzelczyk, W. Drachsel, and H. Weiss, Surf. Sci. **601**, 4843 (2007).
[10] Y. Suchorski, R. Wrobel, S. Becker, and H. Weiss, J. Phys. Chem. C **112**, 20012 (2008).
[11] C. Hardacre, G. M. Roe, and R. M. Lambert, Surf. Sci. **326**, 1 (1995).
[12] K.-D. Schierbaum, Surf. Sci. **399**, 29 (1998).
[13] U. Berner and K.-D. Schierbaum, Thin Solid Films **400**, 46 (2001).
[14] U. Berner and K.-D. Schierbaum, Phys. Rev. B **65**, 235404 (2002).
[15] D. C. Grinter, R. Ithnin, C. L. Pang, and G. Thornton, J. Phys. Chem. C **114**, 17036 (2010).
[16] C. Breinlich, J. M. Essen, E. Barletta, and K. Wandelt, Thin Solid Films **519**, 3752 (2011).
[17] S. Ma, J. Rodriguez, and J. Hrbek, Surf. Sci. **602**, 3272 (2008).
[18] R. Wrobel, Y. Suchorski, S. Becker, and H. Weiss, Surf. Sci. **602**, 436 (2008).
[19] F. Šutara, M. Cabala, L. Sedláček, T. Skála, M. Škoda, V. Matolín, K. C. Prince, and V. Cháb, Thin Solid Films **516**, 6120 (2008).
[20] T. Staudt, Y. Lykhach, L. Hammer, M. A. Schneider, V. Matolín, and J. Libuda, Surf. Sci. **603**, 3382 (2009).
[21] D. R. Mullins, P. V. Radulovic, and S. H. Overbury, Surf. Sci. **429**, 186 (1999).
[22] M. Alexandrou and R. M. Nix, Surf. Sci. **321**, 47 (1994).
[23] S. Eck, C. Castellarin-Cudia, S. Surnev, M. G. Ramsey, and F. P. Netzer, Surf. Sci. **520**, 173 (2002).
[24] J.-L. Lu, H.-J. Gao, S. Shaikhutdinov, and H.-J. Freund, Surf. Sci. **600**, 5004 (2006).
[25] H. Nörenberg and G. A. D. Briggs, Phys. Rev. Lett. **79**, 4222 (1997).
[26] H. Nörenberg and G. A. D. Briggs, Surf. Sci. **402–404**, 734 (1998).
[27] F. Esch, S. Fabris, L. Zhou, T. Montini, C. Africh, P. Fornasiero, G. Comelli, and R. Rosei, Science **309**, 752 (2005).
[28] M. Alfredsson and C. R. A. Catlow, PhysChemChemPhys. **4**, 6100 (2002).
[29] Z. Yang, Z. Lu, and G. Luo, Phys. Rev. B **76**, 075421 (2007).
[30] Z. Yang, Z. Lu, G. Luo, and K. Hermansson, Phys. Lett. A **369**, 132 (2007).
[31] E. L. Wilson, R. Grau-Crespo, C. L. Pang, G. Cabailh, Q. Chen, J. A. Purton, C. R. A. Catlow, W. A. Brown, N. H. de Leeuw, and G. Thornton, J. Phys. Chem. C **112**, 10918 (2008).
[32] Z. Lu and Z. Yang, J. Phys. Condens. Matter **22**, 475003 (2010).
[33] C. Jung, H. Tsuboi, M. Koyama, M. Kubo, E. Broclawik, and A. Miyamoto, Catal. Today **111**, 322 (2006).
[34] Y. Ito, C. Jung, Y. Luo, M. Koyama, A. Endou, M. Kubo, A. Imamura, and A. Miyamoto, Appl. Surf. Sci. **252**, 2598 (2006).

[35]P. Blaha, K. Schwarz, G. K. H. Madsen, D. Kvasnicka, and J. Luitz, *wien2k:An Augmented Plane Wave + Local Orbitals Program for Calculating Crystal Properties* (Vienna University of Technology, Wien, Austria, 2001).
[36]D. J. Singh, Phys. Rev. B **43**, 6388 (1991).
[37]E. Sjöstedt, L. Nordström, and D. J. Singh, Solid State Commun. **114**, 15 (2000).
[38]K. Schwarz and P. Blaha, Comput. Mater. Sci. **28**, 259 (2003).
[39]J. P. Perdew, K. Burke, and M. Ernzerhof, Phys. Rev. Lett. **77**, 3865 (1996).
[40]J. Hubbard, Proc. R. Soc. London **277**, 237 (1964).
[41]V. I. Anisimov, J. Zaanen, and O. K. Andersen, Phys. Rev. B **44**, 943 (1991).
[42]M. Nolan, S. Grigoleit, D. C. Sayle, S. C. Parker, and G. W. Watson, Surf. Sci. **576**, 217 (2005).
[43]M. Nolan, S. C. Parker, and G. W. Watson, Surf. Sci. **595**, 223 (2005).
[44]E. A. Kümmerle and G. Heger, J. Solid State Chem. **147**, 485 (1999).
[45]J. C. Conesa, Surf. Sci. **339**, 337 (1995).
[46]A. D. Mayernick and M. J. Janik, J. Chem. Phys. **131**, 084701 (2009).
[47]A. Kokalj, J. Mol. Graphics Modell. **17**, 176 (1999).
[48]R. F. W. Bader, *Atoms in Molecules - A Quantum Theory* (Oxford University Press, Oxford, 1990).
[49]S. Jenkins, J. Phys. Condens. Matter **14**, 10251 (2002).
[50]S. Jenkins, P. W. Ayers, S. R. Kirk, P. Mori-Sánchez, and A. M. Pendás, Chem. Phys. Lett. **471**, 174 (2009).
[51]S. Imamura, T. Higashihara, Y. Saito, H. Aritani, H. Kanai, Y. Matsumura, and N. Tsuda, Catal. Today **50**, 369 (1999).
[52]S. Penner, D. Wang, D. S. Su, G. Rupprechter, R. Podloucky, R. Schlögl, and K. Hayek, Surf. Sci. **532**, 276 (2003).
[53]S. Penner, G. Rupprechter, H. Sauer, D. S. Su, R. Tessadri, R. Podloucky, R. Schlögl, and K. Hayek, Vacuum **71**, 71 (2003).
[54]M. Fuchs, B. Jenewein, S. Penner, K. Hayek, G. Rupprechter, D. Wang, R. Schlögl, J. J. Calvino, and S. Bernal, Appl. Catal., A **294**, 279 (2005).